Available online at www.sciencedirect.com
ScienceDirect
Journal of Power Sources 176 (2008) 90–95
JOURNAL OF POWER SOURCES
www.elsevier.com/locate/jpowsour

Short communication

Dynamic evaluation of low-temperature metal-supported solid oxide fuel cell oriented to auxiliary power units

Zhenwei Wang [a,*], Jörg Oberste Berghaus [b], Sing Yick [a], Cyrille Decès-Petit [a], Wei Qu [a], Rob Hui [a,**], Radenka Maric [a], Dave Ghosh [a]

[a] *Institute for Fuel Cell Innovation, National Research Council Canada, 4250 Wesbrook Mall, Vancouver, BC, V6T 1W5 Canada*
[b] *Industrial Materials Institute, National Research Council Canada, 75 de Mortagne, Boucherville, Québec, J4B 6Y4 Canada*

Received 21 August 2007; received in revised form 1 October 2007; accepted 2 October 2007
Available online 6 October 2007

Abstract

A metal-supported solid oxide fuel cell (SOFC) composed of a Ni–$Ce_{0.8}Sm_{0.2}O_{2-\delta}$ (Ni–SDC) cermet anode and an SDC electrolyte was fabricated by suspension plasma spraying on a Hastelloy X substrate. The cathode, an $Sm_{0.5}Sr_{0.5}CoO_3$ (SSCo)–SDC composite, was screen-printed and fired *in situ*. The dynamic behaviour of the cell was measured while subjected to complete fuel shutoff and rapid start-up cycles, as typically encountered in auxiliary power units (APU) applications. A promising performance – with a maximum power density (MPD) of 0.176 W cm^{-2} at 600 °C – was achieved using humidified hydrogen as fuel and air as the oxidant. The cell also showed excellent resistance to oxidation at 600 °C during fuel shutoff, with only a slight drop in performance after reintroduction of the fuel. The Cr and Mn species in the Hastelloy X alloy appeared to be preferentially oxidized while the oxidation of nickel in the metallic substrate was temporarily alleviated. In rapid start-up cycles with a heating rate of 60 °C min^{-1}, noticeable performance deterioration took place in the first two thermal cycles, and then continued at a much slower rate in subsequent cycles. A postmortem analysis of the cell suggested that the degradation was mainly due to the mismatch of the thermal expansion coefficient across the cathode/electrolyte interface.

Keywords: Solid oxide fuel cell; Metal-supported; Low-temperature; Dynamic evaluation; Plasma spray

1. Introduction

Solid oxide fuel cells (SOFCs) can convert fossil fuels into electricity in a highly efficient and environmentally friendly way. Over the past two decades, technical developments have focused on both the reduction of the operating temperature and the development of advanced materials to improve the performance and the durability of the cell [1–3]. These efforts are mainly oriented towards stationary applications like centralized power stations or distributed power suppliers. In recent years, however, SOFCs have attracted increasing attention for their potential use as on-board Auxiliary Power Units (APUs) in automobiles and aircraft [4–9]. Such mobile applications require a robust mechanical framework, fast start-up rates, and good resistance to thermal and oxidation cycles in addition to the above-mentioned requirements of long lifetime and high cell performance [1,10,11].

Metal-supported SOFCs have been recognized as a promising replacement for the conventional electrode- or electrolyte-supported SOFCs, based mainly on the following advantages. Firstly, the metal-supported cells with substrates usually made from stainless steels are much more robust than the ceramic of electrolyte-supported cells or the cermet of anode-supported cells. For widely adopted anode-supported SOFCs, the porous Ni-yttria-stabilized zirconia (YSZ) cermet substrate (usually 0.5–1.5 mm in thickness) and the thin YSZ film (thinner than 20 μm) offer relatively low mechanical strength. Structural limitations arise not only from the thermal stress at rapid start-up and during temperature fluctuations, but also from the mechanical stress from assembly compaction and vibrations. In contrast, stainless steel substrates exhibit high mechanical strength, good ductility, and matching thermal expansion coefficient with zirconia and ceria-based electrolytes. Therefore, metal-supported

* Corresponding author. Tel.: +1 604 221 5604; fax: +1 604 221 3001.
** Corresponding author. Tel.: +1 604 221 3111; fax: +1 604 221 3001.
E-mail addresses: Zhenwei.Wang@nrc-cnrc.gc.ca (Z. Wang), Rob.Hui@nrc-cnrc.gc.ca (R. Hui).

0378-7753/$ – see front matter © 2007 Published by Elsevier B.V.
doi:10.1016/j.jpowsour.2007.10.002

SOFCs fulfil the requirements of structural robustness and thermal shock resistance with low internal temperature and stress gradients. Secondly, stainless steels are available commercially in a wide range of compositions and microstructures. The unit price of steel is also at least one order of magnitude lower than that of NiO or YSZ powders; thus, the total material cost can be reduced significantly. Thirdly, metallic substrates can be fabricated into desired shapes, such as planar, circular tubular, and flat tubular by traditional machining. Fourthly, the use of metal substrates can facilitate effective sealing. Glass–ceramic sealants used in electrolyte- and electrode-supported SOFCs need to provide adherence, electrical insulation, chemical stability and compatibility, as well as protection against mechanical degradation from stress during operation. The structural instability resulting from start-up and thermal cycling is usually regarded as one of the main causes of cell breakage and stack failure [12]. Despite the need for inorganic sealants [13] in a metal-supported SOFC stack, the mechanical integrity of the unit cell can be retained even when cracks appear in the sealant. The robustness and the ductility of the steel structure help to alleviate the problems related to the seals, and facilitate the design of SOFC stacks.

Due to these potential merits of metal-supported SOFCs, significant technical progresses have been achieved by the Aerospace Research Center and Space Agency (DLR) [4,14], Ceres Power and Imperial College [13,15], Research Center Jülich (FZJ) [16], and Lawrence Berkeley National Laboratory (LBNL) [17,10]. In our previous study, we reported a metal-supported cell with scandia-stabilized zirconia (ScSZ)/samaria doped ceria (SDC) bi-layer electrolyte fabricated by a combination of pulsed laser deposition (PLD) and wet chemistry processing [18]. The cell showed an open circuit voltage (OCV) of about 1.00 V with promising performance between 400 and 600 °C. Plasma spray processing is an established and cost-effective deposition technique, which offers an alternative method to deposit electrode and electrolyte layers on metal substrates [19]. In this paper, a metal-supported cell composed of a Ni–SDC anode and an SDC electrolyte was prepared by suspension plasma spraying on a porous Hastelloy X substrate. The dynamic behaviour oriented toward APU applications was evaluated and analyzed.

2. Experimental

Porous Hastelloy X was adopted as the metallic substrate, and its basic physical properties are listed in Table 1.

A NiO–SDC anode layer (70 wt.% NiO) was deposited on the porous Hastelloy X substrate (1.25 mm in thickness and 12.7 mm in diameter) by a suspension plasma spray technique. After deposition the anode was reduced in hydrogen for 30 min at 600 °C, thereby inducing the first and possibly most important volume change in the anode. This additional processing step was previously found to reduce crack formation during electrolyte deposition. Some protruding humps on the anode surface, which can sometimes occur in suspension plasma spraying, were removed before subsequent processing. The SDC electrolyte layer was deposited to a thickness of 30 μm while keeping the substrate temperature below 700 °C. An $Sm_{0.5}Sr_{0.5}CoO_{3-\delta}$ (SSCo)–SDC (weight ratio 75:25) composite cathode was screen-printed on the half-cell with an effective area of 0.34 cm^2 and a thickness of 45 μm.

A porous alumina felt was adopted as the sealant on the anode side. Pt meshes were used as current collectors in both the anode and the cathode chambers. More information about the testing setup can be found in our previous work [20]. Prior to testing, the cell was heated to 800 °C and kept at this temperature for 2 h to finish the *in situ* firing of the cathode. To reduce the anode, the cell was then maintained at 650 °C for 5 h while gradually introducing hydrogen. The power generation characteristics were recorded at temperatures from 700 to 400 °C in 50 °C intervals. At each temperature, the electrochemical performance and ac impedance measurements were performed twice using humidified hydrogen as fuel and air as oxidant. Electrochemical performance characteristics were measured using a Solartron 1480A potentiostat with a slew rate of 4 mV s^{-1} in the potential range from OCV to 0.3 V. The ac impedance spectra were obtained in the frequency range of 100 kHz to 0.1 Hz under OCV using a Solartron 1260 frequency response analyzer (FRA) connected to the Solartron 1480A potentiostat.

After the above testing, the cell was kept at 600 °C while completely shutting off the fuel supply such that air could freely diffuse into the anode chamber through the pores of the alumina felt, the Hastelloy X substrate, and the anode layer. After 5 h, the anode chamber was flushed with nitrogen for 30 min, and humidified hydrogen was reintroduced. The power generation characteristics at 600 °C were again recorded.

For the rapid start-up cycles, the cell was cooled to 300 °C at 3 °C min^{-1} in hydrogen, and then cooled to room temperature (RT) in ambient air. The furnace was then reheated to 600 °C at 60 °C min^{-1}. This thermal cycle was repeated 12 times, and the power generation characteristics and ac impedance spectra were recorded after the 1st, 2nd, 4th, and 12th cycles.

Table 1
Physical properties of Hastelloy X

	Ni	Cr	Fe	Mo	Co	W	C	Mn	Si	B
Composition (wt.%)	47[a]	22	18	9	1.5	0.6	0.1	1[b]	1[b]	0.008[b]
TEC		26–649 °C					15.5×10^{-6} K^{-1}			
		26–986 °C					16.6×10^{-6} K^{-1}			
Porosity	27.5% from Archimedes's method									

[a] As balance.
[b] Maximum.

In order to examine the composition and phase of the possible oxide scales on the metallic substrate, Hastelloy X was fired at 900 °C for 3 h in air. X-ray diffraction (XRD) patterns were recorded in the 2θ range of 20–80° with 0.02° step^{-1} using a Bruker D8 Advance diffractometer. To compare the microstructural differences before and after the dynamic evaluation, the cells were vacuum-impregnated with epoxy and the cross-section was polished following standard metallographic procedure. Cross-sectional micrographs were obtained using a scanning electron microscope (SEM, Hitachi S-3500N).

3. Results and discussion

In metal-supported SOFCs, the porous metallic substrate is an integral component to the cell and provides multiple tasks, such as structural support, gas distribution, current collection, and electronic conduction. Fig. 1A shows the cross-sectional image of the metal-supported half-cell without the cathode layer. The Hastelloy X substrate has a porosity of 27.5% and its mean pore size is about 10 μm. The thickness of the anode layer is 20–25 μm and the SDC layer is about 30 μm. Fig. 1B shows a cross-sectional micrograph of the anode and electrolyte layers. A relatively dense electrolyte layer is created. However, some thin vertical defects can be seen in Fig. 1A, which are associated with dark and spongy appearing regions in the anode at the interface. These regions likely represent re-oxidation of the nickel during the spray process, changing the local anode microstructure, which can lead to loss of interface integrity and defect formation. Both layers show intrinsic lamellar structures resulting from plasma spray processing. Although the microstructure is not as fine in the anode and not as dense in the electrolyte as in ones obtained from wet ceramic processing [21], the coatings may provide higher thermal shock resistance due to the additional compliance of the layered structure, impeding the formation of vertical crack.

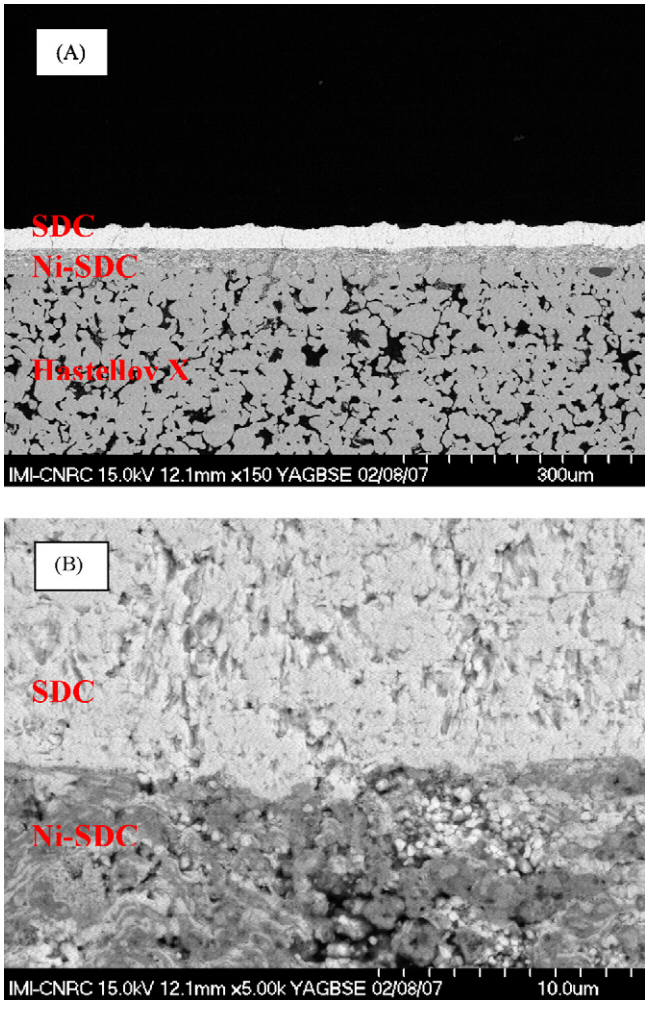

Fig. 1. Cross-sectional SEM image of the metal-supported cell fabricated by plasma spraying. (A) Hastelloy X/Ni–SDC/SDC, ×150; (B) Ni–SDC/SDC, ×5000.

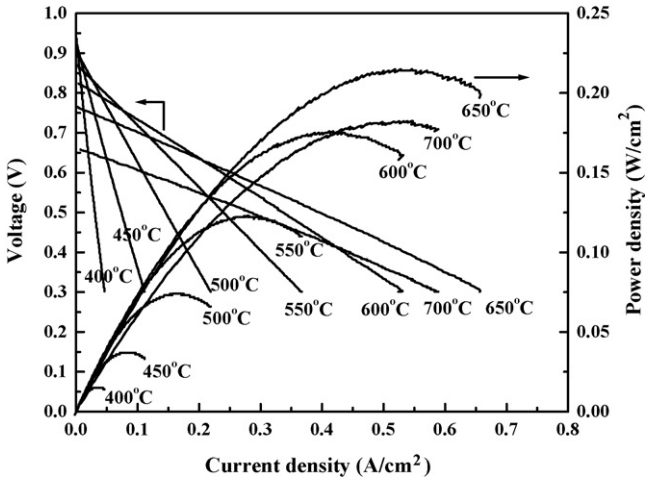

Fig. 2. Power generation characteristics at different temperatures from 400 to 700 °C.

A further benefit may arise from the high nickel content of the substrate. Nickel felt substrate was reported to bring about higher power generation characteristics over other metallic substrates [22,23]. It was believed that the use of Ni metal substrates can enhance the electrochemically active area of the anode for hydrogen reduction.

Fig. 2 shows the power generation characteristics of the metal-supported SOFC tested between 400 and 700 °C. The cell exhibited its highest output at 650 °C, with a maximum power density (MPD) of 0.216 W cm^{-2} and an OCV of 0.768 V. Operated at 700 °C, the cell performance fell noticeably, with an MPD of 0.183 W cm^{-2}, suffering from a serious reduction in OCV to 0.659 V. Fig. 3 gives the OCV values and the area-specific resistances (ASR) at different temperatures. The OCV value decreased slightly at 550 °C (OCV 0.87 V), and then dropped rapidly at higher temperatures. Above 600 °C the electronic contribution to SDC conductivity becomes significant, which leads to current leakage through the electrolyte layer and, in turn, efficiency loss [13]. Similar cell behaviour was observed in an anode-supported cell with a thin SDC film in our previous work [24]. The cell showed an MPD of 0.176 W cm^{-2} at 600°C. This is better than our previously reported metal-supported cell with an ScSZ (2 μm) and SDC (20 μm) bi-layer electrolyte [18], although the previous cell gave an OCV as high as 0.98 V. How-

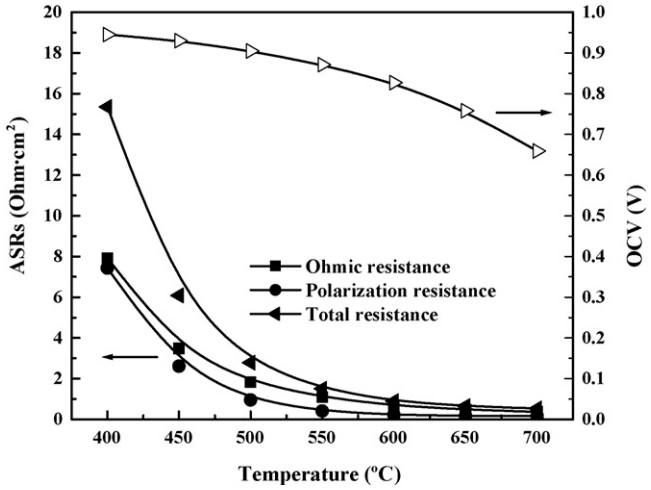

Fig. 3. Resistance and OCV values of the cell under different temperatures.

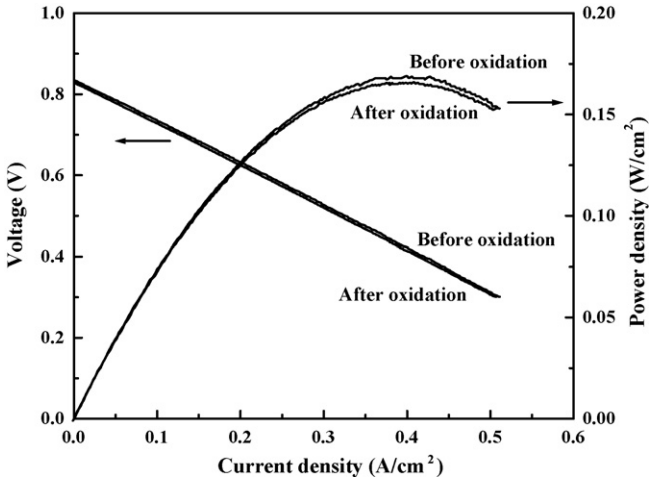

Fig. 4. Comparison of power generation characteristics before and after fuel supply interruption. Hydrogen supply was shut off for 5 h and the cell performances before and after fuel shutoff were tested at 600 °C.

ever, both the ohmic resistance and the polarization resistance in the new cell increased sharply at temperatures below 500 °C, resulting in poor power generation characteristics. In fact, the cell performances at these low temperatures were about 3 times lower than those of the previous metal-supported cell with an ScSZ/SDC bi-layer electrolyte [18]. Besides the thicker SDC layer and the lower OCV, another possible reason is the coarser microstructure in the plasma-sprayed cell, as compared to the PLD-deposited cell, especially in the anode layer. Therefore, further refinement of the microstructure of the plasma-sprayed cell would be promising for operation below 500 °C.

For applications as APUs, accidental fuel shutoff can occur, which can adversely affect the cell performance and irreversibly damage the cell. Volume expansion from Ni re-oxidation may have a significant effect on the integrity of anode/electrolyte interfaces and thus bring about performance degradation [25,26]. In this study, the alumina felt used on the anode side was sufficiently porous for air to diffuse into the anode chamber. In order to facilitate gas exchange in this test, the brim of metal substrate and anode layer was not sealed by any ceramic or glass sealant. The hydrogen flow was stopped for 5 h at 600 °C before recovery. Fig. 4 gives the comparison of the power generation characteristics before the fuel shutoff and after the fuel recovery. A performance loss in MPD of only 1% was observed, which is negligible under practical operating conditions with higher voltages. The cell supported on porous Hastelloy X substrate showed good tolerance against substrate oxidation during the fuel-deficient period.

Fig. 5 compares the XRD patterns of Hastelloy X before and after the oxidation in air. Chromium oxide, Cr_2O_3, appears to be the predominant oxide phase in the metallic substrate, with manganese chromite ($Mn_{1+x}Cr_{2-x}O_4$, spinel) as the minor phase. No nickel oxide could be detected in XRD results. EDX results also show the significant increase of Cr element on Hastelloy X surface. These results are consistent with reports on the oxidation of nickel-based superalloys in air [27] and in humidified hydrogen [28]. The oxidation of Cr and Mn components in air, thermodynamically, are much easier than that of Ni. This is the basic reason that Cr and Mn were preferably oxidized while Ni oxidation was alleviated. When the fuel is shut off and the cell is exposed to air, active Cr and minor Mn species in the Hastelloy X are oxidized firstly. Thus, the Ni component in the Hastelloy X substrate is protected, so drastic volume changes resulting from the Ni re-oxidation in the metallic substrate is avoided. Comparatively, standalone anode samples were significantly cracked suffered from Ni/NiO redox cyclings [25].

Dynamic performance and structural integrity during repeated quick start-ups are a very important issue in APUs. Fig. 6 illustrates the dynamic behaviour of the metal-supported cell during the thermal cycling tests. At a 60 °C min^{-1} heating rate, the cell can reach its working temperature of 600 °C within 10 min. This heating rate is much faster than the 1 °C min^{-1} rate for Integrated Planar SOFCs [11] and the 100–300 °C h^{-1} rate for anode-supported short stacks [29]. This heating rate is even higher than the 50 °C min^{-1} rate adopted for metal-supported SOFCs with YSZ electrolytes [10], considering the

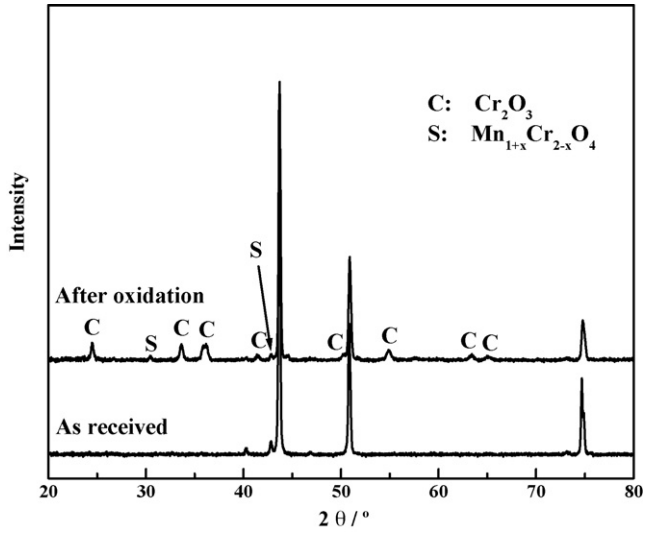

Fig. 5. XRD patterns of Hastelloy X before and after oxidation. Oxidation of Hastelloy X was carried out at 900 °C for 3 h in air.

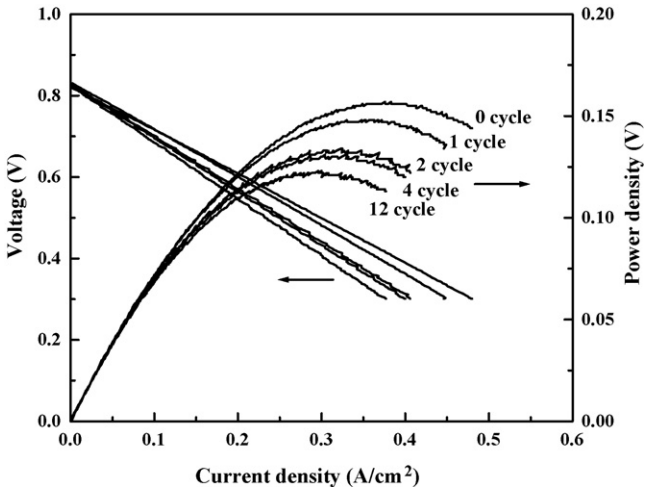

Fig. 6. Power generation characteristics measured at different thermal cycles between 600 °C and room temperature.

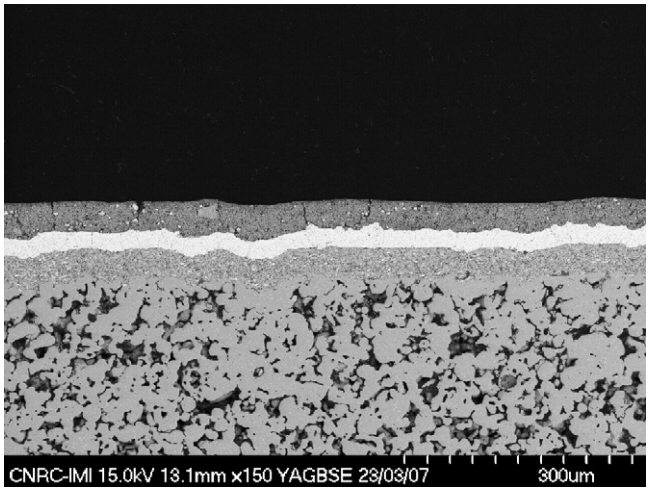

Fig. 8. Cross-sectional SEM image of the metal-supported SOFC after testing.

much stronger mechanical properties of YSZ over SDC. The power generation characteristics show a serious degradation after 12 cycles of quick start-up and cooling. The MPD at 600 °C drops from 0.157 to 0.123 W cm^{-2}, a 15% decline overall. Fig. 7 shows the trends of OCVs and ASRs during these quick start-up cycles. The OCV values remain relatively constant throughout. The polarization resistance increased after the first two cycles and then levelled off, while the ohmic resistance kept climbing slowly after the initial increase in the first two cycles. The simultaneous rise in ohmic resistance and polarization resistance during the first two cycles suggests the presence of cathode delamination [30].

In postmortem analysis, the cross-sectional image of the metal-supported cell after testing is shown in Fig. 8. Compared to Fig. 1A, the microstructures of both anode and electrolyte layers do not change visibly after 12 quick start-up cycles. The cracks in the SDC layer do not widen or increase in number after the tests. This is consistent with the stable OCV, as demonstrated in Fig. 7. The thermal expansion coefficient (CTE) of

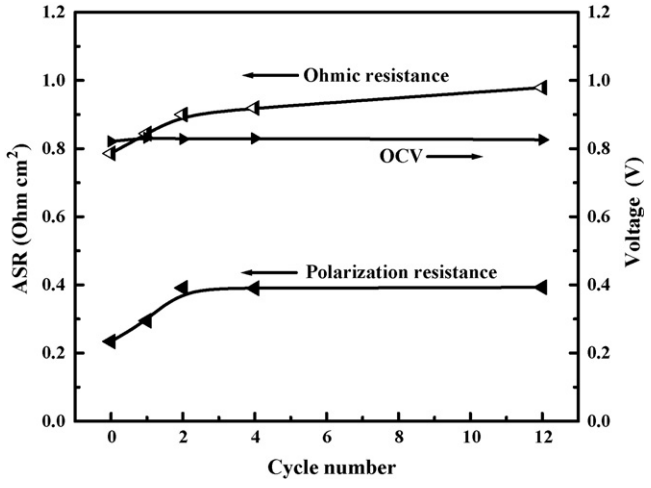

Fig. 7. Resistance and OCV values of the cell measured after different thermal cycles between 600 °C and room temperature.

Hastelloy X is 15.5×10^{-6} K^{-1} between room temperature and 600 °C. This is not much higher than that of the Ni–SDC anode (13.2×10^{-6} K^{-1}, calculated from weight percent) and the SDC electrolyte (12.7×10^{-6} K^{-1}). Such gradual decrease in CTE from substrate to electrolyte reduces thermal stress, avoiding the development of cracks. On the other hand, cracks are found in the cathode layer of SSCo–SDC. Note that the calculated CTE for the SSCo–SDC cathode is about 18.4×10^{-6} K^{-1} (calculated from weight percent), which is much higher than that of its immediate SDC neighbour. Therefore, the thermal expansion mismatch between the SDC layer and the SSCo–SDC composite cathode could be a major factor in the deterioration of performance during the first two quick start-up cycles. Cathode materials with high activity and low TEC for low-temperature operation need to be developed, although the two criteria work against each other in most cases.

4. Conclusions

A metal-supported SOFC with a Ni–SDC anode and an SDC electrolyte were deposited on a Hastelloy X substrate via suspension plasma spraying. The cell showed promising power generation characteristics and good oxidation resistance in air after complete fuel shut off and recovery. The cell was also subjected to rapid start-up cycles at a heating rate of 60 °C min^{-1} from room temperature to 600 °C. Performance deterioration was pronounced during the first two cycles. The degradation can be attributed to the thermal expansion mismatch across the cathode/electrolyte interface. Therefore, cathode materials with a CTE significantly lower than SSCo should be developed to improve the cell's ability to withstand quick start-up cycles, as typically found in APU applications. Moreover, the parameters for plasma spray processing must be further improved to produce anodes with a more refined microstructure, as well as electrolytes that are both thinner and much denser, to improve the cell performance in the low temperature range of around 500 °C. According to the results of the dynamic evaluation, the metal-supported plasma-sprayed cell shows promising prospects for APU applications between 500 and 600 °C.

Acknowledgements

Thanks to the National Fuel Cell and Hydrogen Program of the National Research Council of Canada for the financial support of this work.

References

[1] B.C.H. Steele, A. Heinzel, Nature 414 (2001) 345–352.
[2] Z. Shao, S.M. Haile, Nature 431 (2004) 170–173.
[3] Z. Wang, M. Cheng, Y. Dong, M. Zhang, H. Zhang, Solid State Ionics 176 (2005) 2555–2561.
[4] G. Schiller, T. Franco, M. Lang, P. Metzger, A.O. StÖrmer, Electorchem. Soc. Proc. 07 (2005) 66–75.
[5] M. Stelter, A. Reinert, B.E. Mai, M. Kuznecov, J. Power Sources 154 (2006) 448–455.
[6] J. Lawrence, M. Boltze, J. Power Sources 154 (2006) 479–488.
[7] T. Aicher, B. Lenz, F. Gschnell, U. Groos, F. Federici, L. Caprile, L. Parodi, J. Power Sources 154 (2006) 503–508.
[8] S. Jain, H.Y. Chen, J. Schwank, J. Power Sources 160 (2006) 474–484.
[9] N. Lu, Q. Li, X. Sun, M.A. Khaleel, J. Power Sources 161 (2006) 938–948.
[10] Y.B. Matus, L.C.D. Jonghe, C.P. Jacobson, S.J. Visco, Solid State Ionics 176 (2005) 443–449.
[11] W. Bujalski, J. Paragreen, G. Reade, S. Pyke, K. Kendall, J. Power Sources 157 (2006) 745–749.
[12] S.C. Singhal, Solid State Ionics 152–153 (2002) 405–410.
[13] P. Attryde, A. Baker, S. Baron, A. Blake, N.P. Brandon, d. Corcoran, D. Cumming, A. Duckett, K. El-Koury, D. Haigh, M. Harrington, C. Kidd, R. Leah, G. Lewis, C. Matthews, N. Maynard, T. McColm, A. Selcuk, M. Schmidt, R. Trezona, L. Verdugo, Electrochem. Soc. Proc. 07 (2005) 113–122.
[14] G. Schiller, T. Franco, R. Henne, M. Lang, R. Ruckdäschel, Electrochem. Soc. Proc. 16 (2001) 885–894.
[15] R.T. Leah, N.P. Brandon, P. Aguiar, J. Power Sources 145 (2005) 336–352.
[16] D. Stöver, D. Hathiramani, R. Vaßen, R.J. Damani, Surf. Coat. Technol. 201 (2006) 2002–2005.
[17] S.J. Visco, C.P. Jacobson, I. Villareal, A. Leming, Y. Matus, L.C.D. Jonghe, Electrochem. Soc. Proc. 07 (2003) 1040–1050.
[18] S. Hui, D. Yang, Z. Wang, S. Yick, C. Decès-Petit, W. Qu, A. Tuck, R. Maric, D. Ghosh, J. Power Sources 167 (2007) 336–339.
[19] R. Hui, Z. Wang, O. Kesler, L. Rose, J. Jankovic, S. Yick, R. Maric, D. Ghosh, J. Power Sources 170 (2007) 308–323.
[20] D. Yang, X. Zhang, S. Nikumb, C. Decès-Petit, R. Hui, R. Maric, D. Ghosh, J. Power Sources 164 (2007) 182–188.
[21] Z. Wang, M. Cheng, Y. Dong, M. Zhang, H. Zhang, J. Power Sources 156 (2006) 306–310.
[22] G. Schiller, T. Franco, R. Henne, M. Lang, P. Szabo, Electrochem. Soc. Proc. 07 (2003) 1051–1058.
[23] M. Lang, T. Franco, R. Henne, P. Metzger, G. Schiller, S. Ziehm, Electrochem. Soc. Proc. 07 (2003) 1059–1067.
[24] X. Zhang, M. Robertson, C. Decès-Petit, Y. Xie, R. Hui, S. Yick, E. Styles, J. Roller, O. Kesler, R. Maric, D. Ghosh, J. Power Sources 161 (2006) 301–307.
[25] D. Waldbillig, A. Wood, D.G. Ivey, Solid State Ionics 176 (2005) 847–859.
[26] A. Atkinson, S. Baron, N.P. Brandon, A. Esquiro, J.A. Kilner, N. Oishi, R. Rudkin, B.C.H. Steel, Fuel Cell Sci., Eng. Technol. (2003) 499–505.
[27] D.M. England, A.V. Virkar, J. Electrochem. Soc. 146 (1999) 3196–3202.
[28] D.M. England, A.V. Virkar, J. Electrochem. Soc. 148 (2001) A330–A338.
[29] M. Molinelli, D. Larrain, N. Autissier, R. Ihringer, J. Sfeir, N. Badel, O. Bucheli, J. Van herle, J. Power Sources 154 (2006) 394–403.
[30] J.I. Gazzarri, O. Kesler, J. Power Sources 167 (2007) 430–441.